Nanoscale

Accepted Manuscript

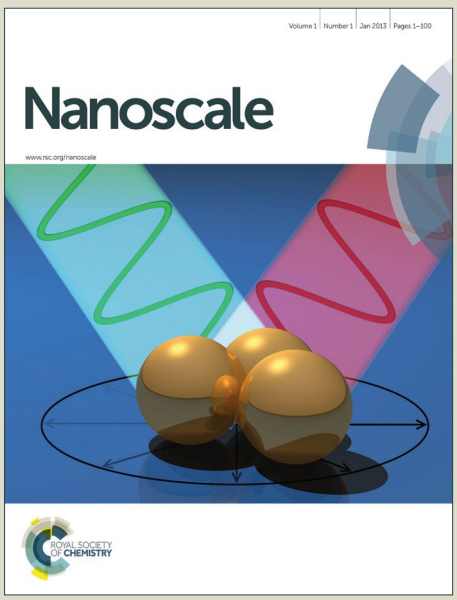

ROYAL SOCIETY OF CHEMISTRY

www.rsc.org/nanoscale

Self-Powered Flexible Fe-doped RGO/PVDF Nanocomposite: An Excellent Material for Piezoelectric Energy Harvester

Sumanta Kumar Karan[1], Dipankar Mandal[2], Bhanu Bhusan Khatua[1,*]

[1]Materials Science Centre, Indian Institute of Technology Kharagpur, Kharagpur 721302, India.

[2]Organic Nano-Piezoelectric Device Laboratory, Department of Physics, Jadavpur University, Kolkata 700032, India.

[*]Corresponding Author: Dr. B. B. Khatua (E-mail: khatuabb@matsc.iitkgp.ernet.in)

Materials Science Centre, Indian Institute of Technology Kharagpur, Kharagpur-721302, India

Tel: 91-3222-283982.

Abstract

In this work, we report superior piezoelectric energy harvester ability of non-electrically poled Fe-doped reduced graphene oxide (Fe-RGO)/poly(vinylidene fluoride) (PVDF) nanocomposite film prepared through an simplest solution casting techniques that favors nucleation and stabilization of ≈ 99% relative proportion of polar γ-phase. The piezoelectric energy harvester was made with non-electrically poled Fe-RGO/PVDF nanocomposite film that gives an open circuit output voltage and short circuit current up to 5.1 V and 0.254 μA by repetitive human finger imparting. The improvement of output performance resembles the generation of electroactive polar γ-phase in PVDF due to the electrostatic interaction among the $–CH_2–/–CF_2–$ dipoles of PVDF and delocalized π-electrons and remaining oxygen functionality of Fe-doped RGO via ion-dipole and/or hydrogen bonding interaction. Fourier transformed infrared spectroscopy (FT-IR) confirmed the nucleation of polar γ-phase of PVDF by electrostatic interaction and Raman spectroscopy also supported the molecular interaction between the dipoles of PVDF and Fe-doped RGO nanosheets. In addition, the nanocomposite shows higher electrical energy density of ≈ 0.84 J/cm^3 at an electric field of 537 kV/cm, indicates appropriate for energy storage capabilities. Moreover, the surface of the prepared nanocomposite film is electrically conducting and shows an electrical conductivity of ≈ 3.30×10^{-3} S.cm^{-1} at 2 wt% loading of Fe-RGO.

Keywords: PVDF, Fe-doped RGO, Polar γ-phase, Self-Powered Device, Energy Density, Piezoelectric Energy Harvester.

Introduction

Due to the growing population, global warming and energy crises, development of renewable, cost effective and green energy technique to convene energy demands for the future generation is the most serious challenges.[1] However, there are various types of energy such as, light, thermal and chemical energy are available in our living environment but the mechanical energy is the most abundant energy in our surrounding due to its greater availability in anywhere and anytime.[2] Hence, self-powdered technology is the great interest to overcome these types of difficulty where no battery component is required (need to link up with vibration/pressure based energy harvester devices with the need of self-power). Recently the self-powered piezoelectric devices with polar electroactive PVDF films became greater attention due to its amazing electroactive properties, such as piezoelectricity, ferroelectricity and pyroelectricity with vulnerable harvesting application.[3] Due to these properties, applications of PVDF have been increased enormously in various fields such as sensor, actuator, non-volatile memories, nanogenerator, biomedical and energy harvester.[3–6] The remarkable progress in the portable electronic devices, the steady reduction of the operating voltage, weight, size of the devices opening the prefeasibility for self-powered electronic devices. For the past 30 years, the energy harvest from environmental noise, fiction, biomedical, thermal and mechanical deformation (low frequency) are of become interest due to its larger impact in the energy sectors.[7] A number of attempted has been taken to construct self-powered piezoelectric energy harvesting devices by well grown inorganic nanomaterials and its polymeric composites. Several piezoelectric materials including ZnO,[7] $BaTiO_3$,[8] PZT,[9] $ZnSnO_3$[10] and GaN[11] etc. have been applicable in diverse form. Although they reveal much superior efficiency in energy conversion, however they are cost intensive, toxic and brittle in nature that harassing the environmental condition.

Recently, similar applications with triboelectric based materials are realized. But it has some limitations, e.g., low stability, low durability, industrial packaging problem in open environment due to humidity, and high output voltage that can damage the electronic circuit, producing fire etc., especially where general electronic circuitry required low power.[12,13] Thus, piezoelectric based polymer materials can overcome these limitations, producing desirable open circuit voltage applicable in open/close environment as it can transfer mechanical to electrical energy using an external pressure or vibrations. Therefore, environmentally stable, biocompatible and flexible PVDF nanocomposites having easy preparative method with cost-effectiveness are one of the better alternative ways. The formation of piezoelectric polar polymorph phases in the semi-crystalline thermoplastic PVDF polymer matrix is the key reason behind the piezoelectric energy harvesting property. It is well known that, PVDF is the most favorable piezoelectric polymer due to its highest piezoelectric co-efficient among the currently available polymers, which are greatly applicable to harvest electrical energy from the mechanical stimuli predominantly applicable in low power and portable electronic devices.[14] Moreover PVDF, being very flexible and does not depolarize under application of high alternating electric field due to its excellent stabilization over long period of time.[15] Conventional piezoelectric properties of PVDF are mainly observed for its β/γ-crystalline polar phase rather other phases.[16] PVDF has mainly four types of phases viz., α, β, γ and δ, represented by the stereo-chemical representation of the structure with alternating s-trans and s-gauche carbon-carbon bond such as TGTḠ, TTTT, $T_3GT_3\bar{G}$, and TGTḠ (polar) (T = trans, G = gauche +, $\bar{G}$ = gauche –), respectively. Among the four phases, β/γ-phase mainly shows valuable piezoelectric property.[17] In addition, the delayed saturation of polarization even at high external electric field enables the γ-phase to exhibit high energy density with high energy storage capacity.[18,19] The γ-phase also shows superior

piezoelectric coefficient like the β-phase, although the latter one is more polar.[20,21] Furthermore, the γ-phase is more environmentally stable compared to the β-phase due to having higher melting temperature that restricts the gradual decaying of the remnant polarization, making it suitable for the production of thermally stable and long-lasting device.[22] But, in order to utilize PVDF in piezoelectric energy harvesting application, the nucleation of γ and β-phases are very essential parameter due to their polar electroactive conformation. Due to stabilization of polar electroactive phase in PVDF, several processes such as mechanical stretching, under electric field and by controlling pressure have been adopted, however, the main problem is that, the quantity of the films and generation of the batch production in industry are not up to the mark for the device production. So, the best alternative way is to add external filler into the PVDF matrix. Recently, nanofillers are in main focus to improve the functionalities of PVDF by stabilizing γ/β-polymorph which is very essential part to improve the piezoelectric energy harvesting property of the PVDF based nanocomposites. Several research groups have attempted to improve the piezoelectric energy harvesting performance by stabilizing electroactive phases by combination of PVDF with fillers such as, graphene,[23] MWCNT,[24] CTAB,[25] graphene-CuS,[26] nanoclay,[27] graphene-ZnO,[28] PMMA-RGO,[29] and Ferrite.[30]

In this study, we report a new, flexible (refer to the Fig. 6E), low cost, light-weight Fe-doped RGO/PVDF (Fe-RGO/PVDF) nanocomposite piezoelectric material prepared through solution casting method. Numerously, Fe-RGO/PVDF nanocomposites film showed high performances of piezosensivity under external repeating pressure where traditional electrical poling is avoided. Graphene and their derivatives have been chosen as conducting nanofiller due to its high surface area and aspect ratio, and superior mechanical, thermal and electrical properties.[31] In addition, Fe-RGO nanofiller have been used as an additive for the nucleation of

the electroactive γ-phase in PVDF, it possibly used for the production of flexible piezoelectric energy harvesting devices, as huge number of vertical compression scheme like, shoes, road transport, bridges, footpaths, tires of vehicle, etc. can be utilized. Besides these properties it is expected that, this composite can be used as tactile sensors, magneto electric material for data storage.[5] The Fe-RGO/PVDF nanocomposite exhibits superior piezoelectric energy harvesting and ferroelectric property where higher proportion polar piezoelectric γ-phase of PVDF is achieved simply by solvent casting method, exclusively produced the output voltage of 5.1 V and short circuit current of 0.254 μA without applying any electrical poling. To the best of our knowledge, no work has been done for the γ-phase stabilization [≈ 99% (± 0.18) of relative proportion] of PVDF applicable as piezoelectric energy harvesting materials using Fe-RGO filler. Furthermore, the touch sensitivity of the un-poled Fe-RGO/PVDF nanocomposite satisfies the great potential feasibility for developing smart sensors for next generation electronic device .[32] The released energy density of ≈ 0.85 J/cm^3 is achieved at 537 kV/cm of electric field which supported that it can be used as effective energy storage material as well. Apart from the increment in piezoelectric property, the presence of conducting Fe-RGO filler in the nanocomposite, it also significantly enhances the surface conductivity up to ≈ 3.30×10^{-3} S.cm^{-1} at 2 wt% of filler loading (see ESI S2.2, Fig. S8, Fig. S9 and Fig. S10).

Materials and method

Materials

Graphite, sodium nitrate ($NaNO_3$), potassium permanganate ($KMnO_4$) and Fe powder (Loba Chemie, India). Graphine oxide (GO) and Fe-doped reduced graphine oxide (Fe-RGO) (laboratory synthesized, the detail procedure and relevant characterization is provided in experiment section of the ESI). (PVDF) (Alfa-Aesar, India). N, N dimethyl formamide (DMF),

hydrogen peroxide (H_2O_2), sulphuric acid (H_2SO_4) and ethanol (C_2H_5OH) (Merck Chemicals, India).

Preparation of Fe-RGO/PVDF nanocomposite film

Fe-RGO was dispersed in DMF (1 mg/ml) using ultrasonicator for 4 h. Separately, PVDF (1 gm) was dissolved in DMF at 90 ºC. The PVDF solution was then mixed with the Fe-RGO solution (mass ratio of Fe-RGO and PVDF ≈ 1: 3) and the resulting solution was kept under ultrasonication for 4 h. Afterwards, the well disperse solution was poured onto petridish and kept in vacuum oven at 120 ^{o}C for 24 h for complete removal of solvent. Finally, dried Fe-RGO/PVDF nanocomposite film (schematically shown in ESI Fig. S1) was obtained. Likewise, different Fe-RGO loading (0.1, 0.5, 1.0 and 2.0 wt%) were prepared and abbreviated as 0.1Fe-RGO/PVDF, 0.5Fe-RGO/PVDF, 1.0Fe-RGO/PVDF and 2.0Fe-RGO/PVDF, respectively.

Characterizations

X-ray diffraction (XRD) measurement were carried out using an X' Pert PRO diffractometer (PAN alytical, Netherland) with nickel-filtered CuKα line (λ = 0.15404 nm) at the scanning rate of 0.25^{o}/min. The characteristic vibrational modes were analyzed by Fourier Transform Infrared Spectroscopy (FT-IR, Jasco FT-IR 300E, ATR mode). Raman spectra were measured using Raman triple spectrometer (T-64000, Horiba-JobinYvon) fitted with a synapse detector. The elemental analysis was analyzed using PHI 5000 Versa Probe II scanning X-ray photoelectron Spectroscopy (XPS) where monochromatic Al Kα source (1486 eV) was employed. The morphological study was carried by FE-SEM through a Carl Zeiss-SUPRA40 FESEM, with an accelerating voltage of 5 kV and transmission electron microscope (JEM-2100, JEOL, Japan) operated at an accelerating voltage of 200 kV. The presence of elements was traced using Energy Dispersive X-ray Spectroscopy (EDS) equipped with FE-SEM and TEM

chamber. Output voltage (piezo-response) was measured using through a digital oscilloscope (Agilent, DS03102A). To collect the mass data of the object (finger) we have used laboratory balance. Applied pressure was calibrated by falling human finger from a certain heights (see electronic supplementary information). The short circuit current was measured using finger imparting through Keithley (model 4200-SCS). The ferroelectric study has been performed using a hysteresis loop tester (Radiant Technologies, Inc, Model 609B). The DC electrical conductivity of the film was evaluated with using four probe techniques. The tensile study was performed using UTM machine (Tinius Olsen H 50 KS). Differential scanning calorimetry (DSC) analysis was carried out for investigation of crystallinity and thermal property using TA instrument (Q20).

Results and discussion

Crystalline phase identification

Formation of crystalline polar γ-phase in the Fe-RGO/PVDF nanocomposite was confirmed by XRD and FTIR analysis. As observed in Fig. 1A, several characteristic diffraction peaks of pure PVDF are observed at 2θ of ≈ 17.6, ≈ 18.3, ≈ 19.9 and ≈ 26.5º are the corresponding reflection planes of (100), (020), (110) and (021) attributing to non-polar α-phase polymorph.[5] However, a more intense single peak is seen at a 2θ ≈ 20.1º in 2.0Fe-RGO/PVDF nanocomposite, corresponds to the diffraction from (002) plane. This peak is the indication for the stabilization of polar γ-crystalline phase of the PVDF in the nanocomposite.[5] The peak intensity of the α-phase (at ≈ 17.6 and ≈ 26.6º) was gradually reduced and becomes invisible with the increasing Fe-RGO loading in the nanocomposite. Another two peaks appeared at ≈ 18.3 and ≈ 19.9º in the nanocomposite are more or less vanished at higher nanofiller loading. This result supported the good interaction between the nanofiller (Fe-RGO) and PVDF matrix. It

also indicates the remarkable conversion of non-polar α-phase crystal to polar electroactive γ-phase crystal (mainly α→γ), which is beneficial for piezoelectric energy harvester and ferroelectric based applications. In addition, the peak appeared at a 2θ ≈ 20.1º is possibly attributed to either γ- or β- or α-phase, i.e., very close to each other and complicated to distinguish from each other by XRD analysis (detailed X-ray pattern of the nanocomposite films is given in ESI Fig. S2(B)). The degree of crystallinity (χ_C) of the nanocomposite was calculated by the following equation:

$$\chi_C = \frac{\sum A_{cr}}{\sum A_{cr} + \sum A_{amr}} \times 100\% \qquad (1)$$

where, $\sum A_{cr}$ and $\sum A_{amr}$ are the summation of integral area of crystalline zone and amorphous zone respectively[33]. It is noteworthy, the crystallinity of PVDF is not changed remarkably, for example, it varies from 42 to 45 % (given in ESI Table S1) with the increasing of filler loading, also verified with DSC analysis (discussed in subsequent section). Due to the heterogeneous nucleation in the presence of Fe-RGO providing by its large surface area for adsorption of the PVDF chain leads to enhance crystallization temperature.

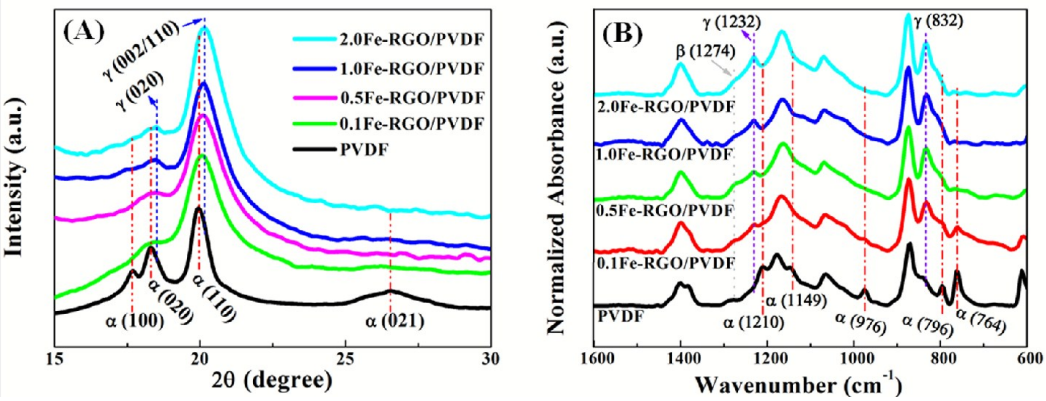

Fig. 1 (A) X-ray diffraction patterns and (B) FT-IR spectra of pure PVDF and Fe-RGO/PVDF nanocomposite at different Fe-RGO loading.

FT-IR spectroscopy gives the detail idea about the exact phase formation of the Fe-RGO/PVDF nanocomposite shown in Fig. 1B. The characteristics absorption bands of non-polar α, polar β and γ-phases of neat PVDF and Fe-RGO/PVDF nanocomposite are observed at 532, 612, 763, 796, 854, 870, 974, 1146, 1210, 1383 and 1423 cm^{-1} for α- phase; 510, 840, 1274, 1286, 1431 cm^{-1} for β-phase and 812, 833, 838 and 1233 cm^{-1} for γ-phase.[5,34] Generally, in most of the cases, absorption bands of β and γ-phases PVDF are superimposed due to common TTT confirmations which created difficulty in phase separation among them.[35] It is noteworthy, in Fe-RGO/PVDF nanocomposite, there is distinct phase separation between the β- and γ-phases is observed where characteristic sharp peaks for the γ-phase appeared at 832 and 1232 cm^{-1}. Pure PVDF exhibits non-polar crystalline α-phases along with very small amount of γ-phase with a broad absorption band at ≈ 838 cm^{-1}. This polar polymorph γ-phase predominantly obtained with the gradual addition of Fe-doped RGO (Fe-RGO) in the PVDF. However, non-polar α-phase with the absorption band at 764, 796 and 976 cm^{-1} are present to some extent in the nanocomposite when it was made with 0.1 wt% filler loading of Fe-RGO. The insufficient stabilization of the γ-crystalline phases at lower loading of Fe-RGO is the key reason behind that. The sharp absorption band peaks are appeared at 832 cm^{-1} and 1232 cm^{-1} with the incorporation of very small amount of Fe-RGO (0.5 wt %) in the nanocomposite which indicated the nucleation and stabilization of electroactive γ-phase beside the sensitive peak of non-polar α-phase. Beyond certain filler concentration (above 0.5 wt%), the absorption intensity of non-polar α-phase gradually decreases while the intensity of γ-phase becomes prominent. Thus, the stabilization of γ-phases becomes more dominant with increasing nanofiller loading in the nanocomposite. In addition, all α-phase characteristic peaks are almost disappeared and γ-phase predominantly visible in the nanocomposite at 1.0 wt% loading of Fe-RGO. So, the

transformation of γ-phase from α-phase occurs gradually with the increasing filler loading and complete conversion of γ-phase was observed at 2 wt% loading of Fe-RGO without appearance of exclusive absorption peak of β-phase (at 1274 cm^{-1}). The 1070 cm^{-1} vibrational band has a linear dependence with the thickness of the nanocomposite film and independent with the crystalline phases of the PVDF. Thus FT-IR absorption is normalized at this peak for the qualitative estimation of α, and γ-phases.[5] FT-IR study reveals that Fe-RGO can stabilize the γ-crystalline polymorph of PVDF and the relative amount of γ-phases was calculated using the following equation: [5]

$$F(\gamma) = \frac{\chi_{(\gamma)}}{\chi_{(\alpha)} + \chi_{(\gamma)}} = \frac{A_{(\gamma)}}{(K_{(\gamma)}/K_{(\alpha)})A_{(\alpha)} + A_{(\gamma)}} \qquad (2)$$

Where, A_α and A_γ represent the absorption intensity of α and γ-phases (at 763 and 832 cm^{-1}), respectively. X_α and X_γ are the corresponding crystallinities of α and γ- phases, respectively. K_α and K_γ are the corresponding absorption co-efficient with the value 0.365 and 0.150 μm^{-1}, respectively.[5,34] The relative proportion of γ-phase ($F_{(\gamma)}$) increases gradually with the increasing of Fe-RGO loading due to the high effective ability of Fe-RGO for the nucleation of electroactive γ-phase (ESI Fig. S11). It reaches a maximum of ≈ 99% (i.e., relative content with respect to other phases present, if any) at 2 wt% of filler loading which is highly suitable for piezo- , pyro- and ferro-electric based sensor and the most importantly piezoelectric energy harvesters. Thus, Fe-RGO/PVDF nanocomposite shows formation of higher content (≈ 99 %) of polar electroactive γ-phase with higher output voltage (discussed in the later section) at such a lower filler loading than ever reported in PVDF nanocomposite with RGO and other nanofillers.[25,36,37] These results emphasized that the Fe-RGO plays an important role for nucleation and stabilization of the γ-phase. This can be explained on the basis of surface charge (developed due to the presence of Fe and/Fe-oxides particles and delocalized π-electrons with

remaining oxygen functionality in RGO) of Fe-RGO and –CH_2–/–CF_2– dipoles of PVDF i.e., presence of electrostatic interaction. The positive charges present in Fe-RGO sheets interact with the –CF_2– dipoles of PVDF segments in the nanocomposite which assisted to stabilize the polar γ-phase by aggregating all locally ordered trans-conformation.

We investigate the asymmetric ν_{as} (–CH_2–) and symmetric ν_s (–CH_2–) stretching vibration bands of PVDF and nanocomposite in the region of 3060 to 2940 cm^{-1} for ensuring any interfacial interaction between the Fe-RGO nanosheets and PVDF matrix. This vibrational band does not coupled with the other vibrational bands. The ν_{as}(–CH_2–) and ν_s(–CH_2–) vibrational bands in the nanocomposite are shifted to the lower frequency region compared to the pure PVDF, indicating the existence of the interfacial interaction among the Fe-RGO and PVDF in the nanocomposites, as shown in ESI in Fig. S12. This shifting of peak position gradually increases with the increasing of Fe-RGO loading due to damping oscillations of –CH_2– dipoles. The effective mass of –CH_2– dipoles of PVDF increased due to the electrostatic interaction among the –CH_2– dipoles and existence of charge into the Fe-RGOs surface. The damping is the effective reasons of decreasing the vibrational frequency of the –CH_2– vibration. The damping coefficient (r_{dc}) has been calculated by considering the shifting of ν_{as}(–CH_2–) vibrational band with the help of the following equation:[33]

$$r_{dc} = 4\pi c(\bar{\nu}^2_{PVDF} - \bar{\nu}^2_{Fe-RGO/PVDF})^{1/2} \quad (3)$$

where, c is the velocity of light. $\bar{\nu}^2_{PVDF}$ and $\bar{\nu}^2_{Fe-RGO/PVDF}$ are the wave number of damping free oscillation of –CH_2– group of neat PVDF and damping containing –CH_2– group of Fe-RGO/PVDF nanocomposites, respectively. The damping co-efficient was accelerated with the variation of Fe-RGO loading which gradually increases with the filler loading and remains

almost constant at 1 and 2 wt% of filler loading, as shown in Fig. 2A. This may happen due to the percolation effect of the Fe-RGO concentration within the PVDF matrix.

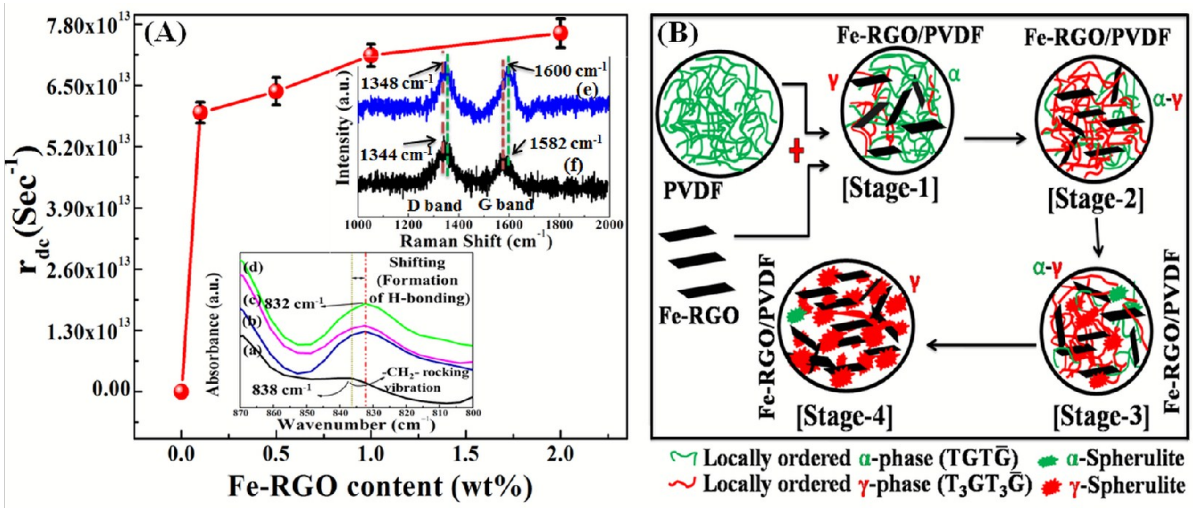

Fig. 2 (A) Variation of damping co-efficient with the filler concentration and (B) Schematic diagram of crystallization of γ- phase in PVDF matrix in the presence of filler. The inset of Fig. 2A shows FT-IR spectra of (a) PVDF, (b) 0.5Fe-RGO/PVDF, (c) 1.0Fe-RGO/PVDF, (d) 2.0Fe-RGO/PVDF in the region of 870 – 800 cm^{-1} and Raman spectra of (e) 2.0Fe-RGO/PVDF nanocomposite film and (f) Fe-RGO.

It is clearly shown that, the damping co-efficient has direct relation with behavior of γ-phase formation due to the electrostatic interaction of the $-CH_2-$ dipoles with the existence charge of the Fe doped RGO nanosheets. In nanocomposite, PVDF chain tried to attract some part and repelled other part due to the ion-dipole interaction which resulted formation of γ-phase. The probable γ-phase nucleation and stabilization due to electrostatic interaction is schematically shown in Fig. 2B. The formation of γ-phase can be described by stage wise, in 1st stage locally ordered γ-phase starts to form from α-phase with the formation of locally ordered α-phase. In 2nd stage, with the adding of more filler the content of γ-phase increases and more number of γ-crystal transforms from α-crystal due to the much more filler effect. In the 3rd step all locally

ordered γ-phase aggregates and forms spherulite type crystals, which is necessary for piezoelectric property. In last stage, with the adding more filler all the ordered γ aggregates and almost completely transforms to spherluite crystal.

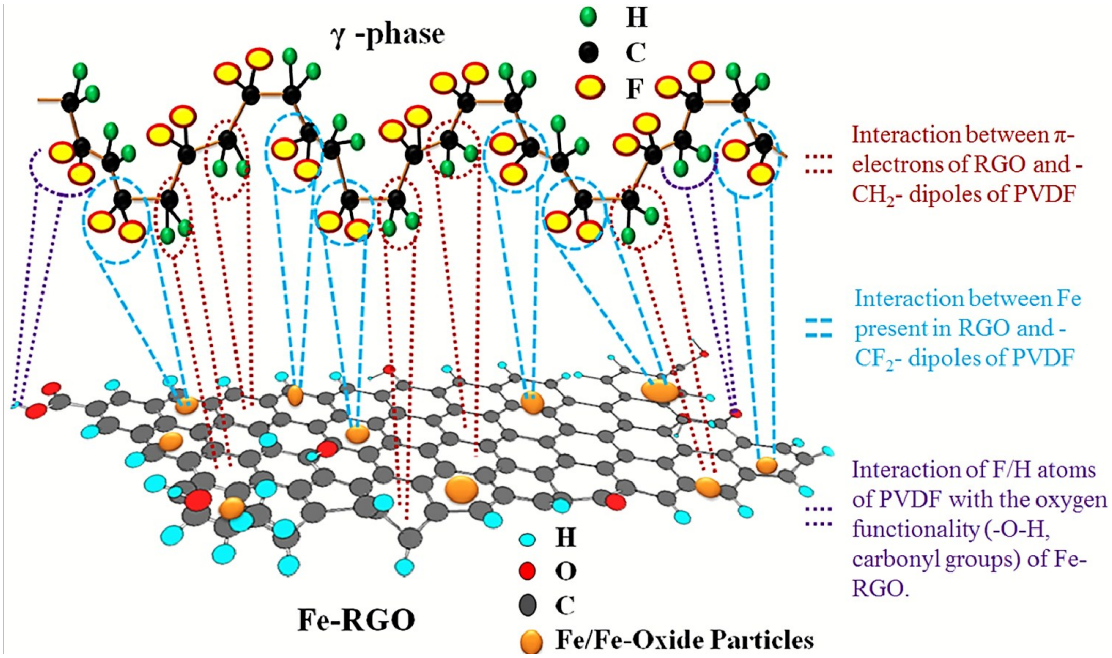

Fig. 3 Proposed schematic illustration showing the interaction between the γ-phase of PVDF and Fe-RGO nanosheet (by assuming single γ-phase and Fe-RGO sheet) facilitating the γ-phase formation within the polymer nanocomposite.

We assume that the probable interaction between the Fe doped RGOs and γ-phases of PVDF leads to the formation of electroactive γ-phase which is schematically shown (considering single γ-phase and Fe-RGO sheet) in Fig. 3. The formation of electroactive γ-phase may interact with the $–CH_2–$/$–CF_2–$dipoles of PVDF and Fe-RGOs, containing Fe and/iron oxides particles. In this case, some $–CH_2–$ dipoles are attracted by the delocalized π-electrons in RGO (gauche conformation) and some $–CH_2–$ dipoles are repelled (trans) by Fe and/iron oxides particles presented in the RGOs, respectively. In another way, some $–CF_2–$ dipoles are attracted (gauche conformation) by Fe and/iron oxides particles and some $–CF_2–$ dipoles repelled (trans

conformation) by delocalized π-electrons of RGOs, respectively. As a result, the γ-phase in the Fe-RGO/PVDF nanocomposite gets stabilized. It may be possible that, the F/H atoms of PVDF are attracted by the functionalities (–OH, carbonyl groups etc.) presents in Fe-RGOs via hydrogen bonding (Fig. 2A inset).

The interaction between the Fe-RGOs and PVDF was also confirmed from Raman spectroscopy (inset Fig. 2A (e,f) and ESI Fig. S4). As can be seen, G band value is largely shifted from 1583 cm^{-1} to 1600 cm^{-1} for 2.0 Fe-RGO/PVDF nanocomposites which clearly supported the strong interaction among PVDF and Fe-RGO nanosheets. However, the I_D/I_G ratio (1.05) slightly decreases with respect to Fe-RGO, which indicates small restoration of hexagonal network structure in the nanocomposites. Thus, due to the presence of charge dissimilarity in the Fe-RGO/PVDF nanocomposites, some $–CH_2–/–CF_2–$ dipoles are attracted and some $–CH_2–/–CF_2–$ dipoles are repelled, that results in the formation of γ-phase.

Thermal analysis

The piezoelectric property of polymer nanocomposites strongly depends on the crystalline structure of the polymer, as well as, on the electroactive polar phase formation in the nanocomposite.[33,35] The melting temperature (T_m) and crystallization temperature (T_c) gradually increase (ESI Table S2) in the nanocomposite with the increase of filler loading (Fig. 4). This is because of homogeneous dispersion of Fe-RGO throughout the matrix, which acts as nucleating agent and inhibits the movement of polymer chain segments, leading to an increase in the T_c value of the nanocomposite.[38,39]

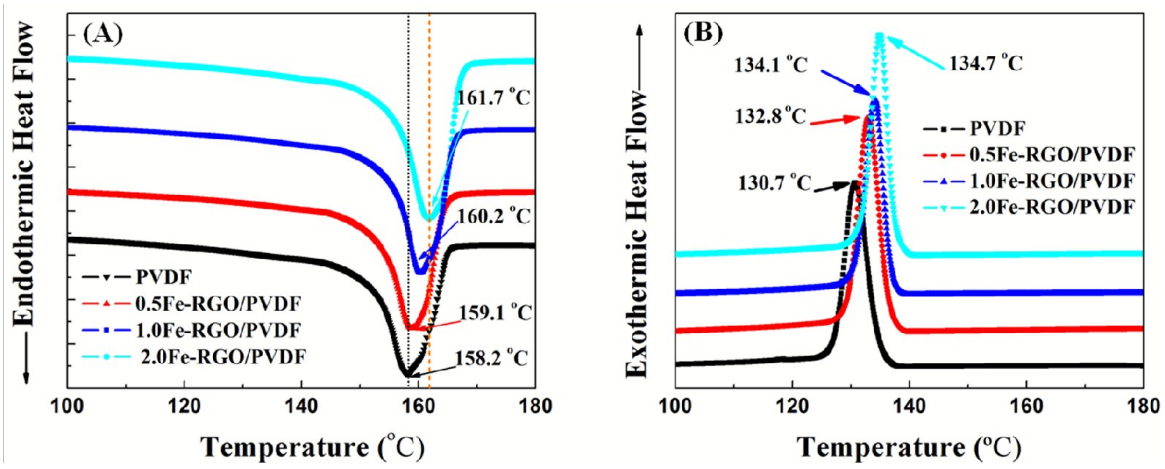

Fig. 4 DSC second melting (A) and cooling curve of pure PVDF and Fe-RGO/PVDF nanocomposite at various Fe-RGO concentrations.

In another way, Fe-RGO induces heterogeneous nucleation by providing its large surface area for adsorption of PVDF chains, which accelerate the nucleation process, as well as, crystallization temperature.[39] The percent crystallinity (χ_c) was calculated using the following equation:

$$\chi_c(\%) = \frac{\Delta H_m}{(1-\phi)\Delta H_m^0} \times 100\% \qquad (4)$$

where, ΔH_m is the melting enthalpy of the nanocomposite, ΔH_m^0 is the melting enthalpy of the 100% crystalline PVDF (104.50 J/g) and ϕ is the weight percentage of the Fe-RGO in the nanocomposite.[40] In our study, we calculated the crystallinity from DSC analysis (listed in ESI Table S2), and found that the crystallinity is not effected remarkably, for example χ_c is 40% in pure PVDF, whereas 45% in 2.0Fe-RG/PVDF nanocomposite.

Furthermore, output performance (piezoelectricity) of the nanocomposite depends on the extent of polar crystalline phase (here γ-phase). During the filler addition, the relative percent of

γ-phase in PVDF progressively increases, and maximum extent of γ-phase formation was achieved at 2 wt% of the Fe-RGO loading.

Surface morphology

The homogeneous dispersion and presence of filler throughout the nanocomposite is clearly seen in the Fig. 5A and Fig. 5B. Fe-RGOs developed a continuous conducting interconnected network path throughout the nanocomposite due to the homogeneous dispersion of the filler. Thus, nanocomposite shows higher sensitivity and surface conductivity even at low nanofiller loading.

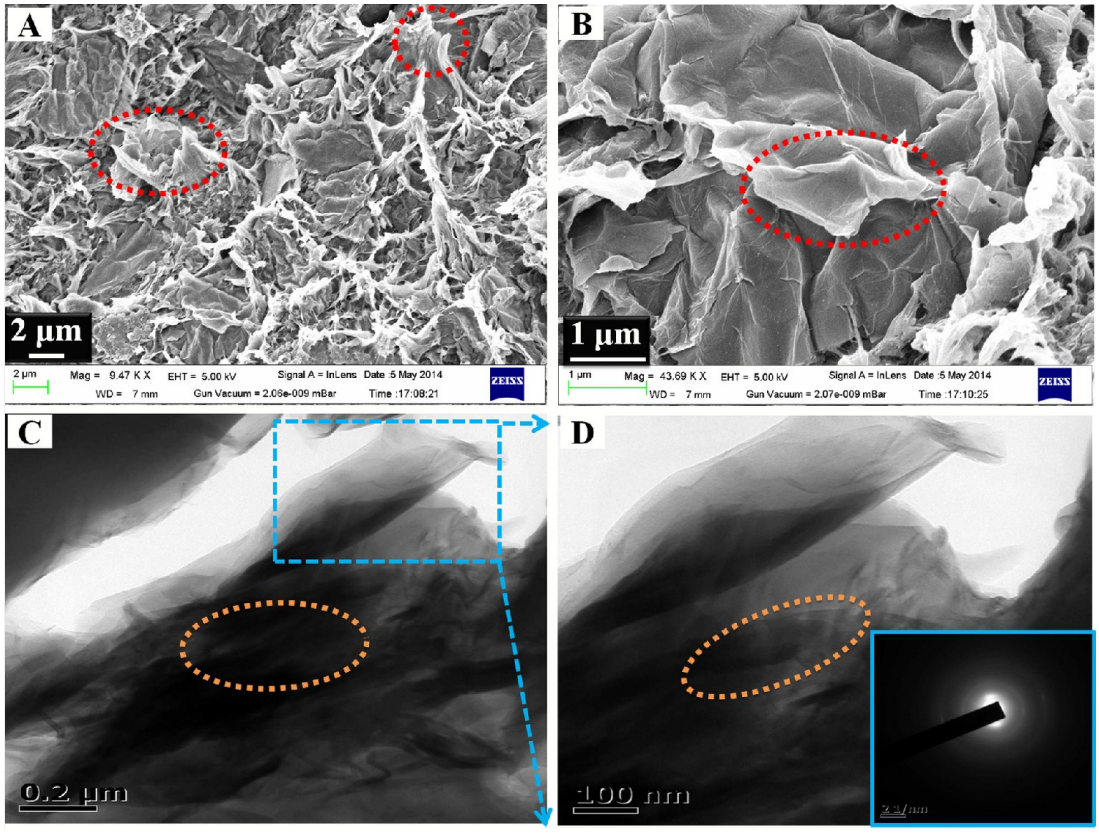

Fig. 5 FESEM images of fracture surface morphology of (A and B) 1.0Fe-RGO/PVDF nanocomposite and HRTEM images of (C and D) 1.0Fe-RGO/PVDF nanocomposite at different resolution respectively. The inset shows the SAED pattern of 1.0Fe-RGO/PVDF nanocomposite.

In another characteristic phenomenon also be found that the Fe-RGO sheet wrinkled, crumbled and even folded/encapsulated within the polymer matrix (shown as red circular dotted line). This type of phenomenon implies that there may be occurrence of interlocking of Fe-RGO nanosheets with the polymer matrix resulting strong bonding interaction between the filler and polymer matrix. From the X-ray mapping (ESI Fig. S5(C, D, E, F)) and EDAX analysis (ESI Fig. S6 and Fig. S7), we confirmed about the presence of the elements of C, O and Fe in the Fe-RGO nanocomposite, respectively. During reduction of GO in presence of Fe/HCl, Fe particles (≈ 1 atomic wt% from XPS spectroscopy) are present as Fe and /Fe-oxides particles on the surface of Fe-RGO which is very well supported by Fig. S5(F) (ESI).

The layer types of morphology of Fe-RGO (ESI Fig. S5) may affect the many properties of nanocomposite. From Fig. 5C and Fig. 5D, it is clearly revealed that layer morphology of the nanofiller (shown as orange dotted line) are retained in the nanocomposite which are homogeneously dispersed throughout the matrix and form a strong network structure in the nanocomposite. Thus, the uniform dispersion of nanofiller takes part to improve the sensitivity and conductivity (surface) of the nanocomposite. This conductivity helps to drain the charges in the nanocomposite film that can improve the device performance. Moreover, the SAED pattern of 1.0Fe-RGO/PVDF nanocomposite has also indicated the semicrystalline nature of the nanocomposite, as shown in inset of Fig. 5D.

Piezoelectric energy harvesting property

To check the piezo-response with energy harvesting capability of the Fe-RGO/PVDF composite films, we fabricated electrode-composite-electrode (ECE) stacks using carbon tape as an electrode (area: 2.0 cm × 3.0 cm) (Fig. 6C). Piezosensing with energy harvesting property of PVDF and Fe-RGO/PVDF nanocomposite films without electrical poling was measured at

different filler loading, via applying mechanical energy by repeated human finger imparting (similar techniques was adopted as demonstrated in video file of ref. 33) onto the upper surface, as shown in Fig. 6. Since, Fe-RGO/PVDF nanocomposite stabilized more polar γ-phase; it exhibits superior piezoelectric property than the virgin PVDF. The expected mechanism of self-powered nanocomposite is the combined effect of Fe-RGO and PVDF. During human finger imparting on the upper surface of the film of ECE stack, the overall charge has been distributed within the whole crystal structure comprising of Fe-RGO and polar electroactive division of the PVDF polymer. As a result, the production of electrical potential difference has been occurred between the two electrodes of Fe-RGO/PVDF film that delivered as open circuit voltage by showing positive and negative amplitude. The positive and negative sign of amplitude indicates the imparting and releasing of human finger from ECE stack, respectively. The maximum open circuit voltage reached up to 5.1 V in 2.0Fe-RGO/PVDF film, (under 12 kPa pressure amplitude, measurement details are given in ESI S2.3), which is about 12 times higher than the virgin PVDF, as shown in Fig. 6. By the application of external pressure, the crystal structures of the Fe-RGO/PVDF film were deformed, resulting strong enhancement in piezo-response by interchanging the deformed structure to stable one or vice-versa.

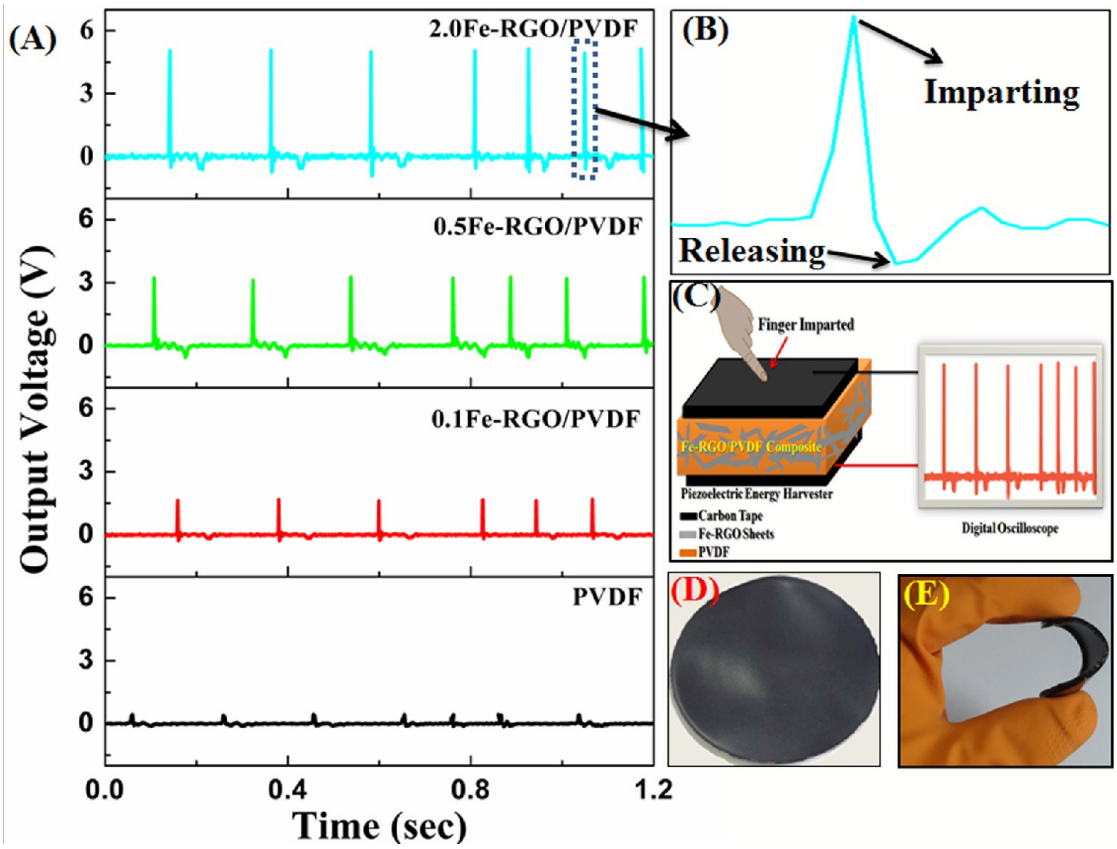

Fig. 6 (A) Output voltage generation (human finger (B) touch and release response) from ECE made with PVDF, 0.1Fe-RGO/PVDF, 0.5Fe-RGO/PVD and 2.0Fe-RGO/PVDF nanocomposite films, and (C) schematic diagram for measuring human finger response signal (Voltage) for Fe-RGO/PVDF film. Photograph of the (D) Fe-RGO/PVDF nanocomposite film and (E) demonstration of the flexibility.

Due to the presence of oppositely charge cloud on the Fe-RGO surface, it actively interacts with the $-CF_2-/-CH_2-$ dipoles of PVDF which promotes the nucleation and stabilization of piezoelectric polar γ-phase by surface charge induced polarization.[41] In addition, by application of external mechanical force on the nanocomposite build a potential in Fe-RGO nanosheets, which can accelerate to align the PVDF dipole further along with the unidirection by stress-induced polarization.[42] As a result, the material gives better piezoelectric output voltage

along with energy harvesting ability. Finally, the dipoles of PVDF molecules are self-polarized along a direction due to the combined effect of stress and surface charge induced polarization without applying any external electric field, resulting formation of self-powered flexible PVDF piezoelectric energy harvester.

During the human finger imparting, the Fe-RGO/PVDF layer experienced a strain upon the surface that produces a deformation in its crystal structure comprises of Fe-RGO and PVDF, leading to the creation of piezo-potential across the surface, contributing the final electrical output signal. This produced piezo-potential on each side on the nanocomposite film induces an inductive charge cloud on the upper and lower electrodes. This potential difference accelerates the flowing of electrons in the external circuit, resulting in the observed output voltage and current. The output voltages of the Fe-RGO/PVDF nanocomposite are nearly symmetrical as typically found in polymer based piezoelectric nanogenerators (NGs).[4,43] As observed from Fig. 7D, the output voltage and short circuit current increased gradually with the increasing of filler loading. However, at 1 and 2 wt% of the filler loadings, the output voltages are nearly same probably due to the percolation effect of nanofiller in the polymer nanocomposite. The maximum obtained output voltage is 5.1V at 2.0 wt% of filler content, which is about 12 times higher than that of virgin PVDF. To the best of our knowledge, this obtained output voltages is significantly higher than ever reported for RGO/PVDF system where typical electrical poling is not applied.[23,44,45] So this type of material can also be used as polymer based nanogenerator (PNG) that may harvest biomechanical energy from human body and promises a wider application as health monitoring systems. In the present study, Fe-RGO/PVDF nanocomposite shows greater touch sensitivity and thus, applicable for touchable sensor such as, footpaths, bridges, shoes, and vehicle and so on. In addition, these types of samples probably give higher output voltages upon

electrical poling, due to presence of more polar phases, which can be used as typical nanogenerator and self-charging battery separator.[46]

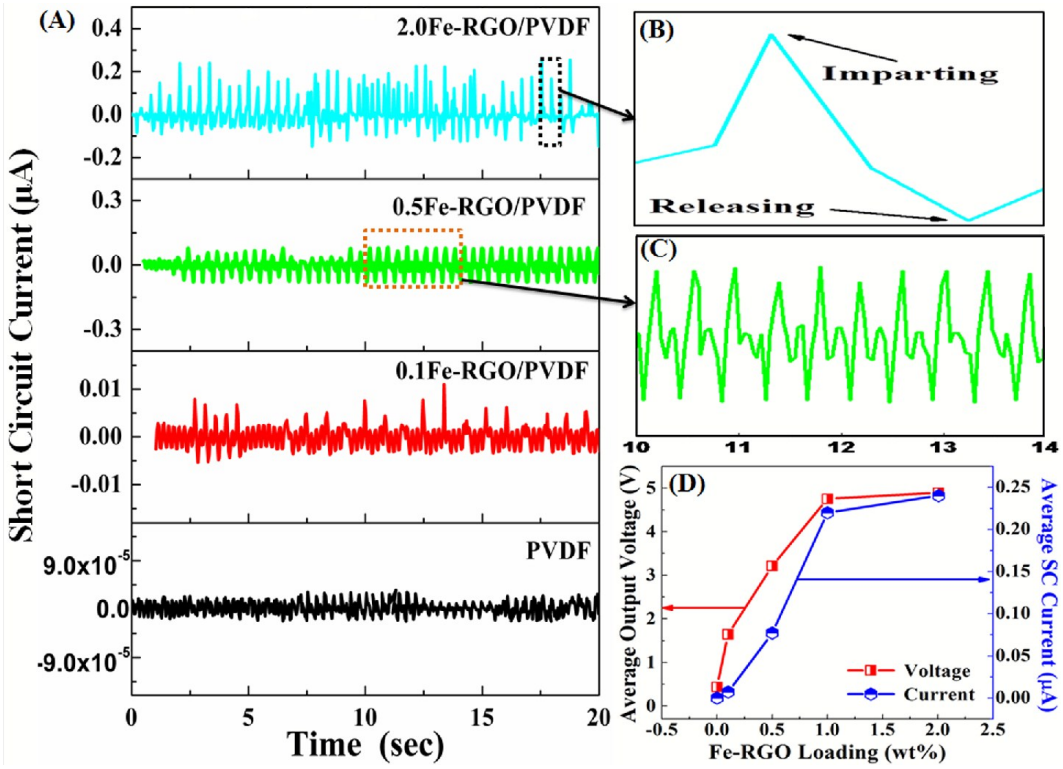

Fig. 7 (A) Generation of short circuit current (during human finger touch and release response (B)) from 0.1Fe-RGO/PVDF, 0.5Fe-RGO/PVDF and 2.0Fe-RGO/PVDF nanocomposite films. (C) Enlarge view of short circuit current in the region of 10–14 sec for 0.5Fe-RGO/PVDF nanocomposite film and (D) the output voltage and short circuit (SC) currents is shown as a function of Fe-RGO filler loading in PVDF.

It has been shown that, (Fig. 7A and 7D) the short circuit current progressively increases with the increasing of filler loading. The maximum short circuit current (alternating current) and output current density of the nanocomposite film reached up to ≈ 0.254 μA and ≈ 0.0422 μA/cm^2 (ESI Fig. S13 and Table S5), respectively, at 2.0 wt% Fe-RGO loading under similar condition (human finger imparting pressure of 12.0 kPa). During the application of mechanical energy, the

film experienced a strain over the surface which deformed the crystal structure of the nanocomposite. At a higher loading, the nanocomposite generates more number of charges due to the presence of more filler content. This charge is easily transferred towards electrodes trough the Fe-RGO network. As a result, the electrodes experience a potential difference which drives the flow of electrons in the external circuit giving as output current (measured at zero voltage), applicable in many electronic devices. The performance of the Fe-RGO/PVDF film provides a new stage for vibration based piezoelectric energy harvester obtainable in human surrounding. Moreover, recently it has been reported that GO acts as self-piezoelectric material,[47] hence it probably influenced the piezoelectric behavior when it is added with other piezoelectric polymer. As RGO is not a fully reduced graphene oxide and contains some oxygen functionality, it also influenced the piezoelectric performance of the nanocomposite. The long term stability of the nanocomposite film is examined over an extended period of time (after 1500 times test) and it gives rise the consistent results. We also examine mechanical test of the nanocomposite film (tensile test) before and after piezoelectric experiments which shows that, the stress-strain behavior (ESI Fig. S14) remains approximately identical after many times of test. Hence, this material demonstrating great promise as a vibration based piezoelectric energy harvester. Moreover, remnant polarization (given in ESI Table S3) is directly proportional to the materials piezoelectric response property. Since, the remnant polarization of Fe-RGO/PVDF nanocomposite is higher than that of PVDF, so output voltages of the nanocomposite will also be high. Thus, nanocomposite has high energy storage capability and becomes superior for piezoelectric energy harvesting application. The values of average maximum output voltage and maximum polarization of PVDF and Fe-RGO/PVDF nanocomposite has been summarized in ESI (Table S3).

Ferroelectric property

Ferroelectric property solely depends on the polar electroactive phases of PVDF which is responsible for piezoelectric energy harvesting behavior of the materials. The ferroelectric domains which are randomly oriented with the electric field in the matrix polymer are greatly responsible for piezoelectric properties.[48] The remnant polarization in the PVDF originally comes from the molecular dipole orientation.[49] The dipoles of the polymer are oriented in a preferred orientation with filler loading, thus, the material shows ferroelectric with piezoelectric behavior. The incorporation of Fe-RGO into PVDF matrix is able to accelerate the internal charge of the nanocomposite which can change the polarization of the material as measured by hysteresis loop measurement (Fig. 8A). A phase separation is observed due to the energy dissipation of the material between the voltage signal and charge. As a result, a loop is formed with the definite area which indicates the charge storage capability of the material. However, the interfacial polarization of the dielectric material occurs due to the swelling of charge at the inner dielectric boundaries of the conductive heterogeneous material. At this condition, fillers are more conducting in nature than the polymer which results the charge mobilization along the particles and facilitates hetero polarization of the material.[50] The polarization gradually increases with the increasing electric field, which indicates that all the molecular dipole are oriented with strong electric field and maximum polarization (about 0.97 μC cm^{-2} at 2 wt% Fe-RGO loading) are obtained at the same electric field. The remnant polarization of 2.0Fe-RGO/PVDF nanocomposite is about 0.167 μC cm^{-2} which is much greater than the pure PVDF (0.044 μC cm^{-2}) at an electric field of 537 kV/cm (measured from Fig. 8A). The change of remnant polarization is probably due to the charge accumulation of molecular dipoles, some strong and specific

interactions of PVDF with the retaining oxygen functionality groups and iron and/Fe-oxide of RGO and necessarily for the hetero polarization.

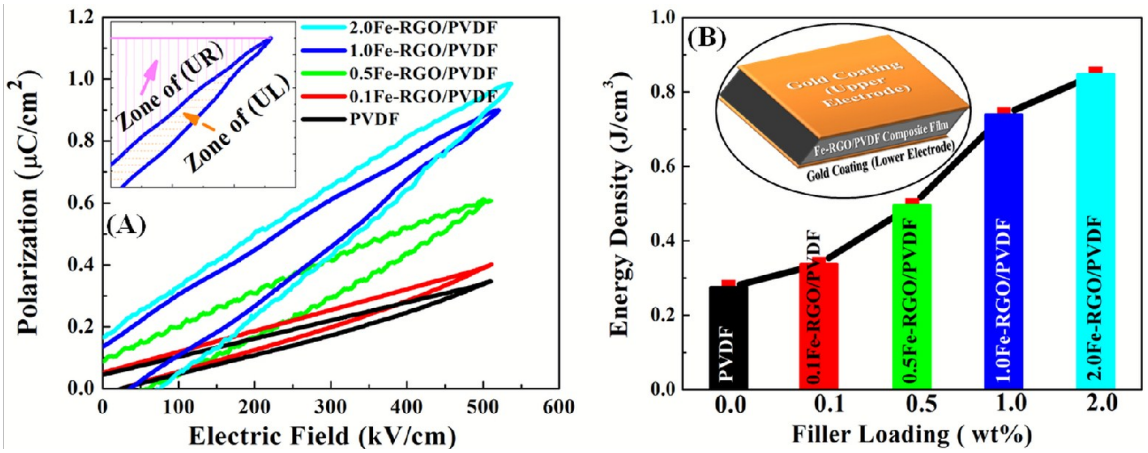

Fig. 8 (A) *P–E* loop of pure PVDF and Fe-RGO/PVDF nanocomposite at different Fe-RGO concentrations (inset shows zone of released energy density (U_R) and loss energy density (U_L)). (B) Variation of released energy density at various filler concentrations. Schematic picture (inset in B) of Fe-RGO/PVDF nanocomposite film for ferroelectric measurement.

The released energy density (U_R) at any electric field can be calculated by integrating the area between the *P–E* loop and the electric field co-ordinate, as shown in inset of Fig. 8A. The energy loss (U_L) is the inside area of the loop and also calculated from *P–E* loop. The total energy density (U_T) stored in the nanocomposite film is the summation of released energy density and the energy loss density of the nanocomposite.

The efficiency of the nanocomposite can be obtained from the ratio between released energy density (U_R) and the total energy density (U_T). As observed in Fig. 8B, the released energy density (0.85 J/cm^3) of the 2.0 Fe-RGO/PVDF nanocomposite is three times greater than (0.27 J/cm^3) the virgin PVDF. The strong interaction among Fe-RGO and PVDF matrix may be the major reason behind the polarization property. The loosing energy density gradually decreases with respect to the released energy density, indicating the material is suitable for high

capacity storage material and thus, it is potential for rechargeable battery industry. The values of U_R, U_L and efficiency of the virgin polymer and polymer nanocomposite are given in ESI (Table S4). These results indicate the presence of interaction of Fe-RGO with the base polymer which can enhance the discharge energy density. The discharge density of the nanocomposite strongly depends on the maximum polarization and lower remnant polarization.[51] Furthermore, enhancement of high energy density is to get high maximum polarization and less remnant polarization which gives more shaded area with more energy density applicable for energy storage materials.

Conclusion

We developed a flexible piezoelectric energy harvesting devices with Fe-RGO nanosheet and PVDF polymer nanocomposite via stabilization of ≈ 99% γ-phases. By simply controlling the filler concentration, almost complete transfer of γ-phases is achieved, as confirmed by spectroscopic and crystallographic studies. Without applying any electric poling Fe-RGO/PVDF nanocomposite gives high output voltage suggesting the possibility of producing a slim, large-scale, lightweight piezoelectric energy harvester of any desirable shape applicable in portable electronic devices. The nanocomposite film exhibited a human finger touch output maximum voltage and short circuit current in the order of 5.1 V and 0.254 μA, which are 12 and 10^5 times greater than the pure PVDF, respectively. It indicates that high level of finger touch sensitivity that possibly can be used in portable electric and electronic devices. Furthermore, presence of high amount of γ-phase of PVDF in the nanocomposite exhibits an energy density of 0.84 J/cm^3 at 537 kV/cm electric field that signifies its applicability as energy storage devices. The superior performance of the piezoelectric energy harvester provides a new platform that might be useful for scavenging energy from environment and also able to store the power.

Acknowledgements

The authors would like to acknowledge financial support from the DST, Govt. of India and providing the INSPIRE fellowship (IF130632). We are also grateful to Mr. Sujoy Kumar Ghosh, Md. Mehebub Alam for helping FT-IR and piezo-response measurement. The authors also thank Mr. Nilesh Kumar Shrivastava, Mr. Amit Kumar Das and Mr. Ranadip Bera for experimental assistance.

References

1 Z. L. Wang and J. H. Song, *Science*, 2006, **312**, 242–246.

2 Z. L. Wang and W. Wu, *Angew. Chem*., 2012, **51**, 11700–11721.

3 V. Bhavanasi, D. Y. Kusuma and P. S. Lee, *Adv. Energy Mater*., 2014, **4**, 1400723–1400730.

4 B. Saravanakumar, S. Soyoon and S. J. Kim, *ACS Appl. Mater. Interfaces*, 2014, **6**, 13716–13723.

5 P. Martins, A. C. Lopes and S. L. Mendeza, *Prog. Polym. Sci*., 2014, **39**, 683–706.

6 A. J. Lovinger, *Science*, 1983, **220**, 1115–1121.

7 B. Saravanakumar, R. Mohan, K. Thiyagarajan and S. J. Kim, *RSC Adv*., 2013, **3**, 16646–16656.

8 Z. H. Lin, Y. Yang, J. M. Wu, Y. Liu, F. Zhang and Z. L. Wang, *J. Phys. Chem. Lett.*, 2012, **3**, 3599–3604.

9 K. I. Park, C. K. Jeong, J. Ryu, G. T. Hwang and K. J. Lee, *Adv. Energy Mater*., 2013, **3**, 1539–1544.

10 M. M. Alam, S. K. Ghosh, A. Sultana and D. Mandal, *Nanotechnology*, 2015, **26**, 165403.

11 C. T. Huang, J. Song, W. F. Lee, Y. Ding, Z. Gao, Y. Hao, L. J. Chen and Z. L. Wang, *J. Am. Chem. Soc.*, 2010, **132**, 4766–4771.

12 M. L. Seol, J.-H. Woo, D.-I. Lee, H. Im, J. Hur, and Y. K. Choi, *Small*, 2014, **10**, 103887–3894.

13 Z. L. Wang, *Faraday Discuss.*, 2014, DOI: 10.1039/c4fd00159a.

14 H. Kawai, *Jpn. J. Appl. Phys*. 1969, **8**, 975–976.

15 J. Wang, H. Li, J. Liu, Y. Duan, S. Jiang and S. Yan, *J. Am. Chem. Soc*., 2003, **125**, 1496–1497.

16 N. Levi, R. Czerw, S. Xing, D. Iyer and D. L. Carroll, *Nano Lett*., 2004, **4**, 1267–1271.

17 C. C. Hong, S. Y. Huang, J. Shieh and S. H. Chen, *Macromolecules*, 2012, **45**, 1580–1586.

18 W. Li, Q. Meng, Y. Zheng, Z. Zhang and W. Xia, *Appl. Phys. Lett.*, 2010**, 96**, 192905–908.

19 Q. M. Zhang, V. Bharti and X. Zhao, *Science*, 1998, **280**, 2101–2104.

20 M. Li, H. J. Wondergem, M. J. Spijkman, K. Asadi, I. Katsouras, P. W. M. Blom and D. M. de Leeuw, *Nat. Mater*., 2013, **12**, 433–439.

21 M. C. G. Gutierrez, A. Linares, J. J. Hernandez, D. R. Rueda, T. A. Ezquerra, P. Poza and R. J. Davies, *Nano Lett*., 2010, **10**, 1472–1476.

22 M. Li, N. Stingelin, J. J. Michels, M. J. Spijkman, K. Asadi, K. Feldman, P. W. M. Blom and D. M. Leeuw, *Macromolecules*, 2012, **45**, 7477–7485.

23 Alamusi, J. M. Xue, L. K. Wu, N. Hu, J. Qiu, C. Chang, S. Atobe, H. Fukunaga, T. Watanabe, Y. L. Liu, H. M. Ning, J. H. Li, Y. Lif and Y. Zhaog, *Nanoscale*, 2012, **4**, 7250–7255.

24 G. H. Kim, S. M. Hong and Y. Seo, *Phys. Chem. Chem. Phys.*, 2009, **11**, 11506–11512.

25 Y. Li, J. Z. Xu, L. Zhu, H. Xu, M.-W. Pan, G. J. Zhong and Z. M. Li, *Polymer*, 2014, **55**, 4765–4775.

26 X. J. Zhang, G. S. Wang, Y. Z. Wei, L. Guo and M. S. Cao, *J. Mater. Chem. A*., 2013, **1**, 12115–12122.

27 A. C. Lopes, C. M. Costa, C. J. Tavares, I. C. Neves, and S. Lanceros-Mendez, *J. Phys. Chem. C*, 2011, **115**, 18076–18082.

28 B. Jaleh and A. Jabbari, *Appl. Surf. Sci.*, 2014, **320**, 339–347.

29 R. K. Layek, S. Samanta, D. P. Chatterjee and A. K. Nandi, *Polymer*. 2010, **51**, 5846–5855.

30 P. Martins, C. M. Costa, M. Benelmekki, G. Botelho and S. Lanceros-Mendez, *J. Mater. Sci*., 2013, **48**, 2681–2689.

31 A. K. Geim, *Science,* 2009, **324**, 1530–1534.

32 Z. Li, X. Zhang, and G. Li, *Phys. Chem. Chem. Phys.*, 2014, **16**, 5475–5479.

33 S. K. Ghosh, M. M. Alam and D. Mandal, *RSC Adv.*, 2014, **4**, 41886−41894.

34 M. Kanik, O. Aktas, H. S. Sen, E. Durgun and M. Bayindir, *Acs Nano*, 2014, **8**, 9311–9323.

35 D. Mandal, K. Henkel, and D. Schmeisser, *J. Phys. Chem. B*, 2011, **115**, 10567–10569.

36 Y. Li, J. Z. Xu, L. Zhu, G. J. Zhong and Z. M. Li, *J. Phys. Chem. B*, 2012, **116**, 14951−14960.

37 Y. Li, J. Z. Xu, L. Zhu, G. J. Zhong and Z. M. Li, *J. Phys. Chem. B*, 2012, **116**, 14951−14960.

38 K. Yang, H. Xingyi, F. Lijun, H. Jinliang and J. Pingkai, *Nanoscale,* 2014, **6**, 14740-14753.

39 L. Huang, C. Lu, F. Wang, and L. Wang, *RSC Adv.*, 2014, **4**, 45220-45229.

40 L. Wu, W. Yuan, N. Hu, Z. Wang, C. Chen, J. Qiu, J. Ying and Y. Li, *J. Phys. D: Appl. Phys.*, 2014, **47**, 135303.

41 Y. Mao, P. Zhao, G. McConohy, H. Yang, Y. Tong and X. Wang, *Adv. Energy Mater.*, 2014, **4**, 1301624.

42 K. Y. Lee, D. Kim, J. H. Lee, T. Y. Kim, M. K. Gupta and S. W. Kim, *Adv. Funct. Mater.*, 2013, **24**, 37−43.

43 D. Mandal, K. Henkel, and D. Schmeißer, *Phys. Chem. Chem. Phys.*, 2014, **16**, 10403−10407.

44 L. K. Wu, Alamusi, J. Xue, T. Itoi, N. Hu, Y. Li, C. Yan, J. Qiu, H. Ning, W. Yuan and B. Gu, *J. Intell. Mater. Syst. Struct.*, 2014, 1−12.

45 M. A. Rahman, B. C. Lee, D. T. Phan and G. S. Chung, *Smart Mater. Struct.*, 2013, **22**, 085017.

46 Z. Chang, W. Yan, J. Shang and J. Z. Liu, *Appl. Phys. Lett.*, 2014, **105**, 023103.

47 X. Xue, S. Wang, W. Guo, Y. Zhang, and Z. L. Wang, *Nano Lett.,* 2012, **12**, 5048−5054.

48 H. Jaffe, *J. Am. Ceram. Soc.*, 1958, **41**, 494−498.

49 T. Furukawa, M. Date and E. Fukada, *J. Appl. Phys.*, 2008, **51**, 1135−1141.

50 Z. Ounaies, C. Park, K. E. Wise, E. J. Siochi and J. S. Harrison, *Compos. Sci. Technol.*, 2003, **63**, 1637−1646.

51 C. Pecharroman and J. S. Moya, *Adv Mater.*, 2000, **12**, 294−297.